(SUPPORTING INFORMATION)

Excitonic AND Logic Gates on DNA Brick Nanobreadboards

Brittany L. Cannon,[†] Donald L. Kellis,[†] Paul H. Davis,[†] Jeunghoon Lee, [†,‡] Wan Kuang,[§] William L. Hughes,[†] Elton Graugnard,[†] Bernard Yurke,[†,§,*] and William B. Knowlton[†,§,*]

[†] Department of Materials Science and Engineering, [‡]Department of Chemistry and Biochemistry, [§]Department of Electrical & Computer Engineering

(*email: bknowlton@boisestate.edu, bernardyurke@boisestate.edu)

SUPPORTING INFORMATION S1: *Strand Sequences, Schematics, and Chromophore Details*

The sequences for nanobreadboards are given in Table S1 below. Strands (i.e., DNA bricks) are identified according to the nomenclature depicted graphically in Figure S1.1 in which H indicates the helix on which each strand is situated and C corresponds to the column where the crossovers for each strand occurs. For example, H1C1 indicates a strand in which the 5' end originates in helix 1 and the crossover (i.e., section of strand that hybridizes to a neighboring strand) occurs in column 1. The 21 nucleotide (nt) bottom-most strands are labeled according to the column in which the 5' end originates and the 3' end terminates (e.g., H6C(5')-(3')). Injection strands (i.e., T1, T2, I1, I2, R1 and R2) specific to the different logic gate designs are provided separately at the bottom of Table S1. Nanobreadboards with chromophores are assembled by substituting strands with the corresponding chromophore or tether augmented strands. DNA bricks from the nonaugmented nanobreadboard that are substituted are noted in parentheses. All oligonucleotides were purchased from Integrated DNA Technologies.

Figure S1.2 illustrates the strand hybridization and toehold-mediated strand displacement processes for both TAMRA 1 and TAMRA 2, which is the same for both logic gates. Accompanying the schematics are the net free energy values given per strand invasion step. The difference between the net free energies per step provides the driving force for each step in which there is a free energy minimization. The free energy minimization is a combination of enthalpic and entropic reduction due to base pair formation and strand dissociation.

Table S1: DNA nanobreadboard and logic gate sequences

DNA Brick Name	Sequence (5' to 3')	Length (nt)	Purification
Nanobreadboard Strands			
H1C1	CTGAGATGATCTCAAACGAAT	21	Standard Desalting *
H1C2	CCCTTCCCGCCTTAGGCGGCT	21	Standard Desalting
H1C3	CCTGGCTAGTCTATTGTTAAT	21	Standard Desalting
H1C4	CTACGTGGAGCTTTTTTTTTT	21	Standard Desalting
H2C1	TTTTTTTTTTTTACCTTGCTTGATCATCTCAGTTTTTTTTTT	42	Standard Desalting
H2C2	CGCTTAAGTCTTGGCGCTAATGGCGGGAAGGGATTCGTTTGA	42	Standard Desalting
H2C3	CCCTAGGCCCTAGCTGCATGTGACTAGCCAGGAGCCGCCTAA	42	Standard Desalting

H2C4	CTAAGCCTTCTGTTAATTCTTGCTCCACGTAGATTAACAATA	42	Standard Desalting
H3C1	CTTGCTTTGCCTCCTAACGATGACTTAAGCGAAGCAAGGTAA	42	Standard Desalting
H3C2	CAATACACCGCTGCAAGACCTGGGCCTAGGGATTAGCGCCAA	42	Standard Desalting
H3C3	CTTGGGACGGCTTTGGAAATTGAAGGCTTAGACATGCAGCTA	42	Standard Desalting
H3C4	CCAATTAGGACTAATTTAGATGTGGAGCCCGAAGAATTAACA	42	Standard Desalting
H4C1	TTTTTTTTTTTGTTGTTTGTTGGCAAAGCAAGTTTTTTTTTT	42	Standard Desalting
H4C2	CTCTGACGGCTACATTGAGGTGCGGTGTATTGATCGTTAGGA	42	Standard Desalting
H4C3	CGGAAGTGCCTCCATGATTGTGCCGTCCCAAGAGGTCTTGCA	42	Standard Desalting
H4C4	CTACCATGGCTGCTCACGAGTGTCCTAATTGGAATTTCCAAA	42	Standard Desalting
H5C1	CATGCCTGCCCTTGCTAACTTGCCGTCAGAGAACAAACAACA	42	Standard Desalting
H5C2	CAAGACTATACTCAGGACGCTGGCACTTCCGACCTCAATGTA	42	Standard Desalting
H5C3	CACGCGCATCCTCCGTTTATTGCCATGGTAGACAATCATGGA	42	Standard Desalting
H5C4	CGTAAAGCTGCTATGGTCTATGCCGACTAAGACTCGTGAGCA	42	Standard Desalting
H6C1	TTTTTTTTTTTCAGTATGTATGGGCAGGCATGTTTTTTTTTT	42	Standard Desalting
H6C2	CTGTATCGGCTTTAGTATAATGTATAGTCTTGAAGTTAGCAA	42	Standard Desalting
H6C3	CATCTGGGTCTACAAGACCCTGGATGCGCGTGAGCGTCCTGA	42	Standard Desalting
H6C4	CACAGATGTCTATTTGCGAGTGCAGCTTTACGAATAAACGGA	42	Standard Desalting
H6C2-1	GCCGATACAGATACATACTGA	21	Standard Desalting
H6C3-2	GACCCAGATGATTATACTAAA	21	Standard Desalting
H6C4-3	GACATCTGTGAGGGTCTTGTA	21	Standard Desalting
H6C5-4	TTTTTTTTTTACTCGCAAATA	21	Standard Desalting
AND Logic Gate 1 – Augmented Bricks			
FAM (H3C1)**	/56-FAM/ CTTGCTTTGCCTCCTAACGATGACTTAAGCGAAGCAAGGTAA	42	HPLC ***
TAMRA 1 (H4C2)	CTCTGACGGCTACATTGAGGTGCGGTGTATTGATCGTTAGGA•CATCTAAGTGAGTAAC	58	Standard Desalting
TAMRA 2 (H5C2)	CAAGACTATACTCAGGACGCTGGCACTTCCGACCTCAATGTA•TTGGCAATAATTCCGC	58	Standard Desalting
TAMRA 1	GTTACTCACTTAGATG•TAGCATATCG /36-TAMSp/	26	HPLC
TAMRA 2	GCGGAATTATTGCCAAGTCGTGCCAT /36-TAMSp/	26	HPLC
Cy5 (H4C3)	CGGAAGTGCCTCCATGATTGTGCCGTCCCAAGAGGTCTTGCA /3Cy5Sp/	42	HPLC
Invasion 1	AGTAACGGTTCGATATGCTACATCTAAGTG	30	Standard Desalting
Invasion 2	TATTCGCCTTATGGCACGACTTGGCAATAA	30	Standard Desalting
Restoration 1	AGATGTAGCATATCGAACCGTTACT	25	Standard Desalting
Restoration 2	GCCAAGTCGTGCCATAAGGCGAATA	25	Standard Desalting
AND Logic Gate 2 – Augmented Bricks			
FAM (H5C1)	CATGCCTGCCCTTGCTAACTTGCCGTCAGAGAACAAACAACA /36-FAM/	42	HPLC
TAMRA 1 (H4C2)	CTCTGACGGCTACATTGAGGTGCGGTGTATTGATCGTTAGGA•CATCTAAGTGAGTAAC	58	Standard Desalting

TAMRA 2 (H5C2)	CAAGACTATACTCAGGACGCTGGCACTTCCGACCTCAATGTA•TTGGCAATAATTCCGC	58	Standard Desalting
TAMRA 1	GTTACTCACTTAGATGTAGCATATCG /36-TAMSp/	26	HPLC
TAMRA 2	GCGGAATTATTGCCAAGTCGTGCCAT /36-TAMSp/	26	HPLC
Cy5 (H4C3)	CGGAAGTGCCTCCATGATTGTGCCGTCCCAAGAGGTCTTGCA /3Cy5Sp/	42	HPLC
Invasion 1	AGTAACGGTTCGATATGCTACATCTAAGTG	30	Standard Desalting
Invasion 2	TATTCGCCTTATGGCACGACTTGGCAATAA	30	Standard Desalting
Restoration 1	AGATGTAGCATATCGAACCGTTACT	25	Standard Desalting
Restoration 2	GCCAAGTCGTGCCATAAGGCGAATA	25	Standard Desalting

* Desalting to remove short products and small organic contaminants. Does not include PAGE purification.
**Chromophore-functionalized brick substituted for the standard nanobreadboard brick, standard nanobreadboard brick in parentheses
***High-Performance Liquid Chromatography

The common names and sources for the chromophores used in this study are:

FAM: 6-carboxyfluorescein N-hydroxysuccinimide ester.

TAMRA: Xanthylium, 9-[2-carboxy-5-[[(2,5-dioxo-1-pyrrolidinyl)oxy]carbonyl]phenyl]-3,6-bis(dimethylamino)-, inner salt.

Cy5: 1-[3-(4-monomethoxytrityloxy)propyl]-1'-[3-[(2-cyanoethyl)-(N,N-diisopropyl phosphoramidityl]propyl]-3,3,3',3'-tetramethylindodicarbocyanine chloride.

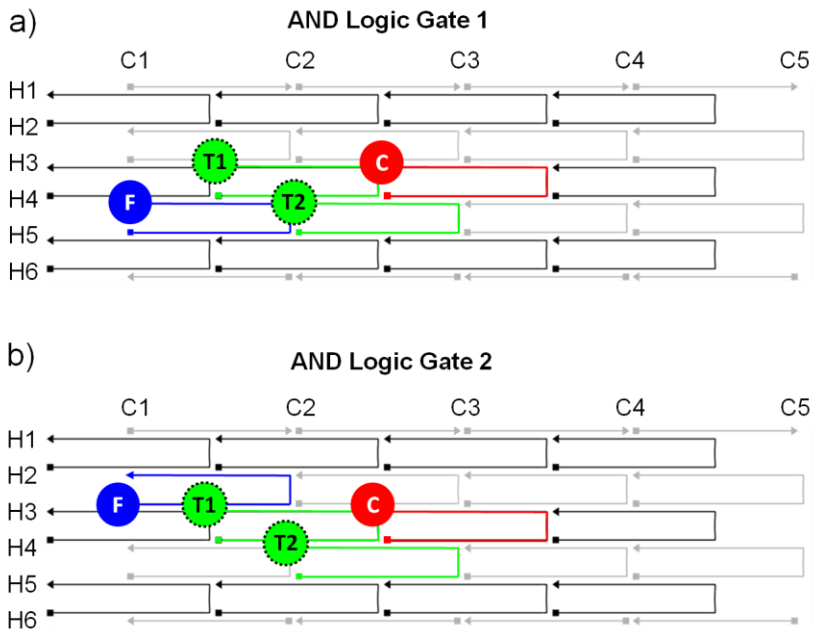

Figure S1.1: Schematic of **(a)** AND logic gate 1 and **(b)** AND logic gate 2 indicating strand position relative to DNA helices (H) 1-6 and crossover columns (C) 1-4. The sequences of the four bottom most strands, also described in Table S1, are labeled according to the column in which the 5' end originates and the 3' end terminates (e.g., H6C(5')-(3')).

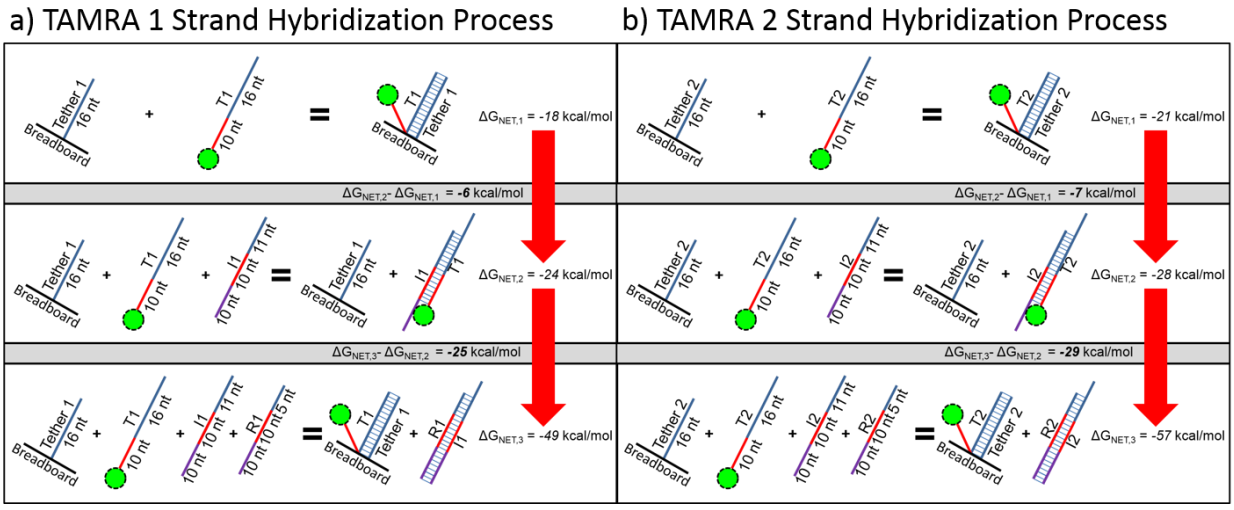

Figure S1.2: Schematic of **(a)** TAMRA 1 and **(b)** TAMRA 2 strand hybridization and toehold-mediated strand displacement processes for a single switching cycle. Each step of the process can be quantified thermodynamically by a net free energy value. The driving force for the logic switching (red arrow) is minimization of the free energy, which can be defined as the change in free energies per logic state.

SUPPORTING INFORMATION S2: *Experimental Methods*

Nanobreadboard Synthesis S2.1: Oligonucleotides for both nanobreadboard designs were purchased lyophilized (Integrated DNA Technologies), rehydrated using ultrapure water (Barnstead Nanopure, Thermo Scientific) and used without further purification. Oligomers purified by the manufacturer are indicated in Table S1. Nanobreadboards were synthesized through directed self-assembly by combining equimolar amounts of oligomers at ~2 μM in a 1×TAE, 15 mM Mg^{2+} (40 mM tris(hydroxymethyl)aminomethane, 20 mM acetic acid, 2 mM ethylenediaminetetraacetic acid and 15 mM magnesium chloride; pH 8.3) solution. TAE (10x stock solution) and magnesium chloride (anhydrous, ≥98% purity) were purchased through Fisher Scientific. Both nanobreadboard designs were synthesized without T1 and T2 attached to the nanobreadboard (OFF-state, Logic Output: 0) to better analyze transmission line and logic gate performance. All nanobreadboards were annealed at 90 °C for 20 min and cooled to room temperature over 22 hours (~0.05 °C/min) using a thermal cycler (Mastercycler Nexus Gradient, Eppendorf).

Amicon Filtration Purification Techniques S2.2: Millipore Amicon Ultra 0.5 mL 100 kDa centrifugal filter units purchased through Fisher Scientific were used for purification purposes to remove excess (i.e., unreacted) bricks. Filters were initially rinsed with 500 μL of 1×TAE buffer (15 mM added $MgCl_2$) and centrifuged at 14k relative centrifugal force (rcf) for 8 minutes using an Eppendorf model 5418 centrifuge. The buffer solution was then removed from the unit and replaced with 500 μL of sample and centrifuged at 14k rcf for 10 minutes. The centrifuged sample was subsequently rinsed by decanting the supernatant and adding an additional 500 μL of 1×TAE buffer (15 mM added $MgCl_2$) to the unit followed by centrifugation at 10k rcf for 10 minutes. The filter was then removed from the unit and inverted to deposit the sample into an empty standard ultra-centrifugation tube to be centrifuged at 1000 rcf for 4 minutes. Recovered samples were collected using a micropipette and the concentration quantified by measuring the absorbance at 260 nm (Biophotometer Plus, Eppendorf). Typical concentrations after purification were ~200 nM. Samples were then diluted to ~25 nM for fluorescence spectroscopy.

Agarose Gel Band Identification S2.3: To aid in the structural characterization of the nanobreadboards and assess the efficacy of Amicon filtration for purification purposes, agarose gel-electrophoresis was used to identify well-formed structures with correct chromophore

arrangements. This approach allows structures to be identified by the emission wavelengths of the individual chromophore types attached to the nanobreadboards.

Samples of nanobreadboards with various chromophore arrangements were mixed in a 5:1 ratio with 6× New England Biolabs loading buffer (1× buffer: 11 mM ethylenediaminetetraacetic acid, 3.3 mM tris-hydrochloric acid, 0.017% sodium dodecyl sulfate, 0.015% bromophenol blue, 2.5% Ficoll®-400), injected into a 1.5% agarose gel, and allowed to run for approximately 120 minutes with a 50 V applied voltage. Completed agarose gel runs were analyzed and imaged using a multiplexed gel imaging and documentation system (FluorChemQ, ProteinSimple).

Figure S2.1 shows images of two different completed gel runs in which wells are located on the left, and DNA migration occurs from left to right. The contents for each lane are indicated on the right of each image. Image **(a)** shows nanobreadboards with individual chromophores (i.e., FAM, TAMRA, or Cy5) in place to provide a standard for band color identification. Image **(b)** shows nanobreadboards with various multichromophore arrangements. Both images were created by overlaying three separate exposures using different excitation and emission filter combinations, as listed in Table S2. Each exposure was chosen to specifically capture the emission from the desired chromophore and mapped to a red, green, or blue channel as indicated. Thus, the bands in the multiplexed image are easily identified via the associated false colors. The left most band in image **(b)** with the light red hue is likely a result of Cy5 emission due to FRET between F and C, crosstalk, and bleedthrough. The left most bands are indicative of well-formed nanobreadboards.

Figure S2.2 shows an image of a completed gel run in which the bottom three lanes show DNA nanobreadboards that have been annealed for 2 hours and Amicon filtered as described in section S2.2. In contrast, the top three lanes show DNA nanobreadboards that have been annealed for 24 hours as described in section S2.1 and Amicon filtered as described in section S2.2. The 2-hour anneal nanobreadboards produced faint bands relative to the 24-hour anneal nanobreadboard bands, suggesting a lower yield of well-formed nanobreadboards. Furthermore, the combination of annealing for 24 hours and Amicon filtering the samples significantly reduced the number of malformed nanobreadboards as compared to the nonfiltered samples shown in Figure S2.1. Though Figure S2.2 shows there remained some malformed nanobreadboards within the Amicon filtered samples that may decrease the threshold tolerance and marginally impair device

performance, we have found that the logic gates are still able to operate as desired. We therefore carried out all fluorescence measurements and switching experiments using Amicon filtered nanobreadboard samples, rather than gel purified samples, to speed the prototyping process.

Table S2: Excitation and emission combinations for chromophore identification

Dye	Excitation Wavelength (nm)	Emission Filter (nm)	Color Channel
FAM	462	537 ± 18	Blue
TAMRA	527	606 ± 34	Green
Cy5	637	699 ± 31	Red

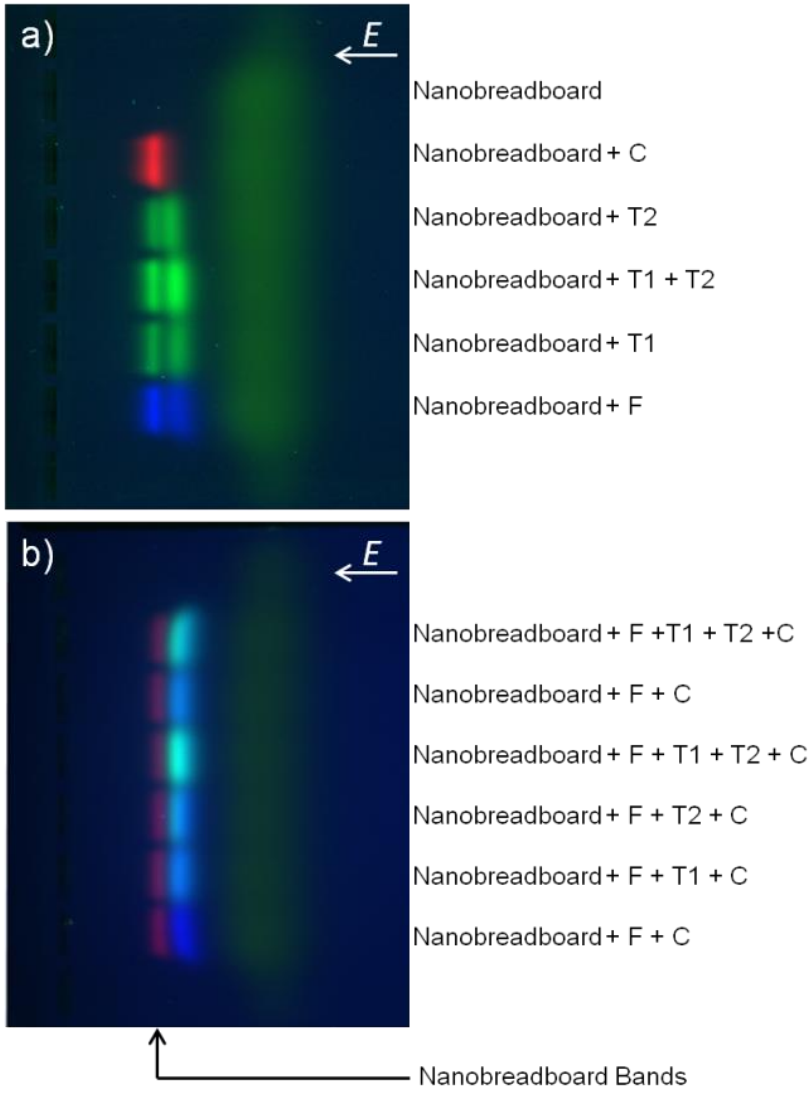

Figure S2.1: Images of two agarose gels containing two-dimensional DNA brick-based nanobreadboards (6 helices x 94 base pair) with various chromophore arrangements. DNA migration occurs from left to right against the flow of electric current towards the positive electrode. Image **(a)** analyzes the chromophore emission of FAM, TAMRA and Cy5 individually, filtered according to Table S2. The lack of a second band within the lane labeled "Nanobreadboard + C" may indicate that most Cy5 augmented strands were successfully assembled within the well-formed nanobreadboards. Image **(b)** examines various chromophore arrangements using the filters given in Table S2 to apply a false color that aids in band identification. The right most bands contain malformed or partially formed nanobreadboards that most likely result from nonstoichiometric strand ratios. The light red hue observed in every left band may suggest direct FRET between F and C, emission of F at the emission filter wavelength, emission of C as a result of direct excitation, or crosstalk from either of the TAMRA chromophores.

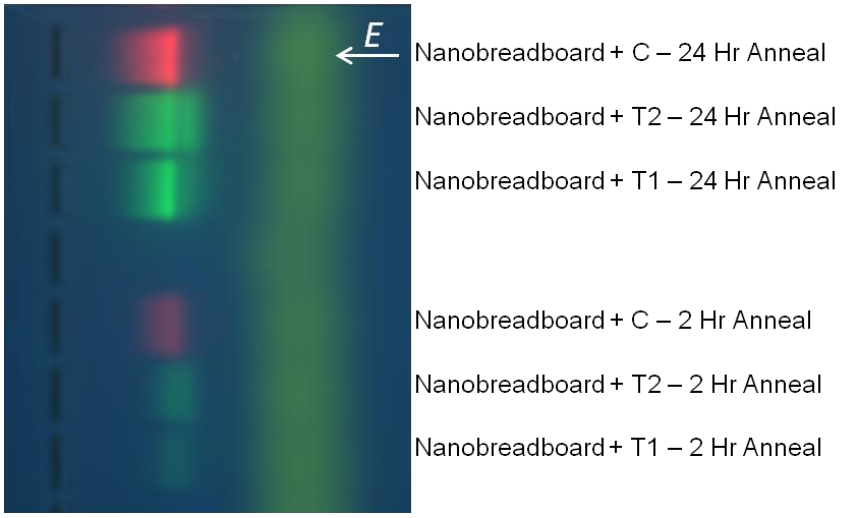

Figure S2.2: Image of an agarose gel containing two-dimensional DNA brick-based nanobreadboards (6 helices x 94 base pair) with various chromophore arrangements that have been Amicon filtered as described in section S2.2. The image has false colors added according to Table S2 to analyze the chromophore emission of FAM, TAMRA and Cy5 individually. The bottom three lanes contain nanobreadboards that have only been annealed for 2 hours and the top three lanes contain nanobreadboards that have been annealed for 24 hours. The top three lanes show nanobreadboards primarily within the left most bands, indicating most nanobreadboards are fully formed and properly assembled.

Atomic Force Microscopy Imaging Techniques S2.4: To verify the size, shape, and structure of assembled nanobreadboards, atomic force microscopy (AFM) images were acquired using Peak Force Tapping™ mode in air on a Bruker MultiMode 8 equipped with a Nanoscope V controller. 5 μL of Amicon filtered sample were pipetted onto a freshly cleaved mica surface, immediately covered with 40 μL of 0.5×TBE (10 mM added $NiCl_2$), and allowed to incubate for approximately 5 minutes to promote adsorption of DNA onto the mica surface. Samples were then blown dry with ultra-high purity (99.999%) N_2 gas (Norco) and imaged using ScanAsyst-Air-HR probes (k = 0.4 N/m, f = 130 kHz) mounted in a ScanAsyst-HR probe holder. Acquired images, such as that shown in Figure S2.3, were analyzed using WSxM 4.0 Beta 6.1[1] and/or Nanoscope Analysis 1.50 imaging software. Image analysis of the nanobreadboards revealed the expected rectangular dimensions of 29.6 ± 2.2 nm x 18.6 ± 1.1 nm with a sample size N = 15.

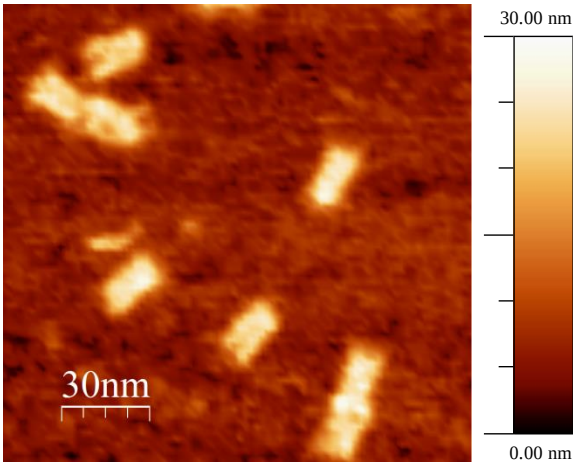

Figure S2.3: 160 nm x 156 nm height image of DNA brick-based nanobreadboards acquired using a MultiMode 8 AFM (Bruker). Image was collected in air and analyzed using WSxM 4.0 Beta 6.1.

Fluorescence Spectroscopy Techniques S2.5: Both fluorescence emission spectra and fluorescence intensity versus time data (i.e., dynamic switching data) were obtained using a Fluorolog-3 Spectrofluorometer (HORIBA Scientific). Absorption spectra were obtained from samples at 5 μM using a Cary 5000 spectrophotometer (Agilent Technologies). To demonstrate nanobreadboard reconfigurability and distinguish between AND logic states, as described in Figure 2a, emission spectra were collected for both logic gate designs with various T1 and T2 arrangements present (See Figure S2.4). Logic gates were excited at 450 nm (F peak absorption). This wavelength was chosen to fall within the excitation band of F while limiting spectral overlap with the absorption bands of T and C to minimize direct excitation of the downstream chromophores in the FRET transmission line (Figure S2.5). The resultant fluorescence emission spectra were acquired and the intensity at 668 nm (C peak emission) monitored to detect changes in FRET intensity with the attachment of T1 and T2. Emission spectra were normalized by nanobreadboard concentration. The normalized output intensities at 668 nm (logic outputs) are shown in Figure 2b, c for the various states of the logic gates.

Fluorescence intensity versus time plots showing sequentially-switchable AND logic gate operations (Figure 3) were obtained by exciting the nanobreadboards at 450 nm. The intensity of the C (logic output) fluorescence emission at 668 nm was monitored as a function of time. The real-time dynamic measurements of AND gate switching provide information regarding FRET

between F and C to give the realtime ON/OFF-state transitions of the gate. Throughout the collection of the dynamic switching data, the solution was held at a constant temperature of 35 °C to promote strand hybridization and diffusion after injections. To initially switch the logic gate from an OFF-state to an ON-state, T1 and T2 chromophore strands were injected independently and the resulting solution was allowed to stand for 20 min at 35 °C to permit hybridization to occur. Cycling between ON- and OFF-states was accomplished through the repeated addition of invasion and restoration strands in equimolar amounts. All dynamic switching emission spectra were normalized by concentration to account for dilution factors resulting from injecting the small volumes of T1, T2, invasion, and restoration strands into the sample solution. Additionally, photobleaching of F led to a decrease in the monitored fluorescence output signal as a function of time and was corrected for as discussed in Section S3 below.

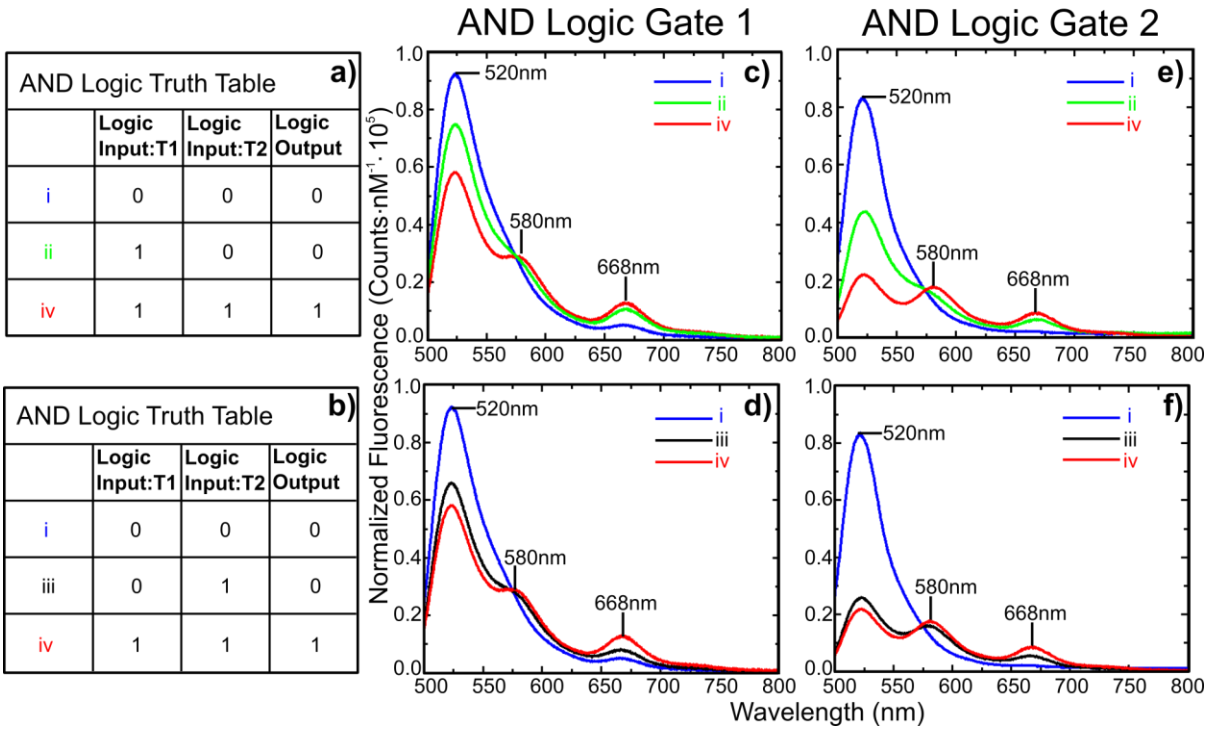

Figure S2.4: AND logic truth tables describing the logic values associated with the ON- (Logic Output: 1) or OFF- (Logic Output: 0) states for the attachment (Logic Input: 1) or displacement (Logic Input: 0) of T1 or T2 onto/from the nanobreadboard where either **(a)** T1 or **(b)** T2 is attached onto the nanobreadboard first. Adjacent to each truth table are fluorescence spectra that correspond to either the attachment of T1 or T2 preceding the other for AND logic gate 1 **(c** and **d)** and 2 **(e** and **f)**. All spectra were collected by exciting F at 450 nm. All strands were added in

solution successively in equimolar amounts and the spectra were normalized by concentration. Figure 3 provides the criteria for assigned logic values.

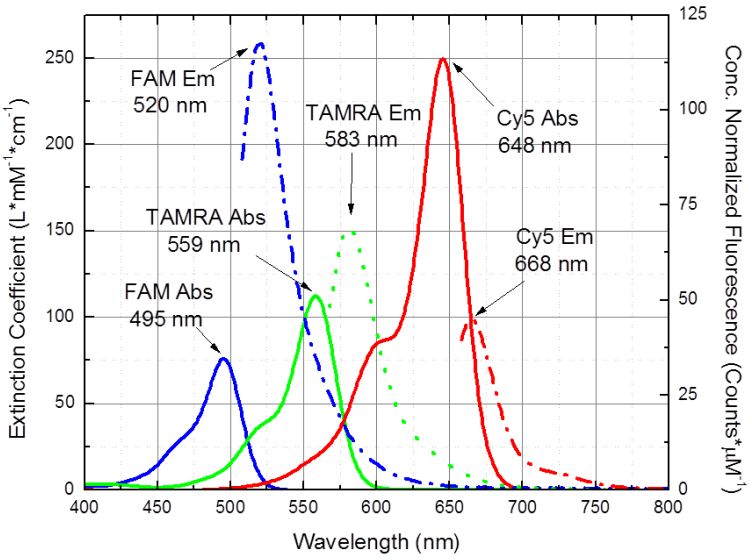

Figure S2.5: Individual extinction coefficient (solid lines) and concentration normalized fluorescence (dashed-dot lines) spectra for FAM (blue), TAMRA (green), and Cy5 (red) overlaid to highlight the spectral overlap. Note that to obtain the fluorescence emission spectra each chromophore was excited at its peak absorbance wavelength.

Mechanical Stability of Nanobreadboards as Modeled by CanDo S2.6: CanDo is computer-aided engineering software that is offered free of charge online at: http://cando-dna-origami.org/. The model shown in Figure S2.6 takes into consideration the effects of entropic elasticity of single-stranded DNA thermal fluctuations. The computational prediction of deformed DNA shapes is performed using the Finite Element Method, which is a well-established numerical technique for the analysis of complex structural mechanics and dynamics. The thermally induced fluctuations of DNA nanostructures are computed using the equipartition theorem of statistical mechanics and normal mode analysis. The false colors represent rms fluctuations in which blue corresponds to smaller fluctuations and red signifies high fluctuations. The predicted nanobreadboard rms fluctuation was a maximum of 1.6 nm. We have designed both of our logic

gates such that the chromophore attachment sites and attachment tethers fall within the higher stability regions (i.e., blue regions) to reduce variations in chromophore distances.

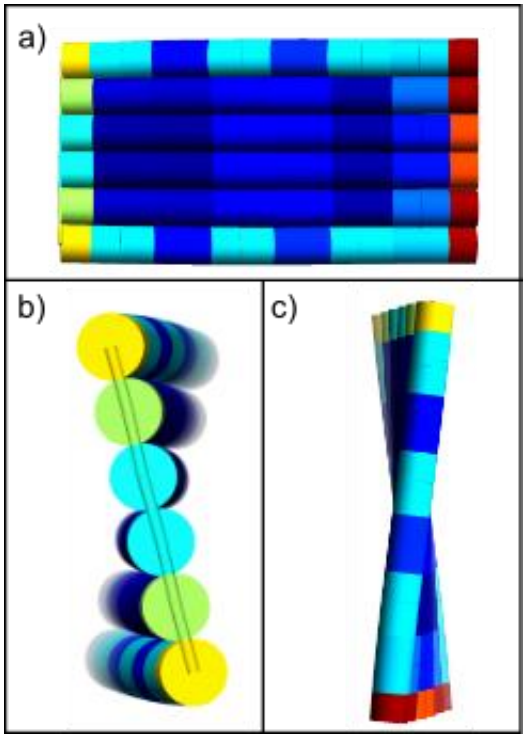

Figure S2.6: Mechanical stability of a DNA brick-based nanobreadboard as modeled by CanDo. Images shown along the **(a)** face, **(b)** end, and **(c)** side views. The colors indicate mechanical structure stability in which red specifies low structural stability and blue indicates high structural stability.

SUPPORTING INFORMATION S3: *Photobleaching and Fluorescence Background Correction Procedure*

Two complicating factors leading to an overall decrease in fluorescence intensity with time were observed in the course of obtaining and analyzing the dynamic switching data (Figure 3).These factors were: (1) serial dilution of the sample with each successive injection arising from the addition of TAMRA, invasion, and restoration strands to the sample solution, and (2) photobleaching of FAM.[2-3]

The fluorescence decrease resulting from dilution factors is readily corrected for by calculating the volumetric and concentration changes as a function of time due to strand injections. This was accomplished by dividing the raw dynamic switching data (Figure S3.1) into time segments based on strand injection times and individually normalizing each section by concentration. This correction process is denoted by:

$$I_c = \frac{I_{668FC,raw}(t)}{[Nanobreadboard](t)}, \quad \text{(S1)}$$

where I_c indicates the corrected data, $I_{668FC,raw}(t)$ is the raw data collected as a function of time, and $[Nanobreadboard](t)$ is the concentration of nanobreadboards in solution at time *t* (taken to be a step function). The outcome of this process is shown in Figure S3.2.

The photobleaching rate of FAM is dependent on the concentration of reactive molecular species present within the buffer, such as oxygen, and to a lesser extent on the presence or absence of Cy5 and/or TAMRA on the nanobreadboard.[2-3] Both the concentration of the reactive molecular species and the chromophores changes over the course of the experiment. The former varies with environmental factors such as the amount of ozone present in the air during sample preparation and is unknown to us; therefore, making an accurate first principles prediction of the photobleaching rate is impractical. Thus, we have instead fit a single-exponential decay function to each of the four dynamic switching data sets individually to obtain an average time-dependent photobleaching rate for each system separately. Hence, the expression for the fluorescence intensity corrected for both complicating factors (i.e., serial dilution and photobleaching) is:

$$I_c = \frac{\frac{I_{668FC,raw}(t)}{[Nanobreadboard]_{FC}(t)}}{I_{668,EDF}(t)}, \quad \text{(S2)}$$

where $I_{668,EDF}(t)$ is the amplitude (intensity) of the exponential decay function as a function of time arising from the fit to the data. This term is inherently normalized for concentration and given in units of counts per nanomolar. Thus, the resultant I_c values are unitless numbers. Fitting parameters for the exponential decay function per panel are given in Table S3. Note that in Figure S3.2, the upper (blue) and lower (red) curves are not true "fits" to the data, but rather were created by scaling the pre-exponential factor appropriately such that the curves pass through the fully ON- or fully OFF- states to guide the eye. The fact that these curves do not perfectly fit the data is likely because the rate of FAM photobleaching is somewhat dependent on the logic state of the nanobreadboard since FRET (i.e., excitonic transmission down the line of chromophores) will shorten the FAM excited state lifetime and hence the likelihood of photobleaching, whereas we are using an average photobleaching rate of all logic states. In addition, we are neglecting differences in reaction rates, which are addressed in greater detail in Section S4.

Figure S3.3 shows the emission of FAM (a), TAMRA (b), and Cy5 (c) as a function of time while being continuously excited at 450 nm, 559 nm, and 648 nm, respectively. As shown in Figure S3.3a, the photobleaching rate of FAM can be fit with an exponential decay function. In contrast, Figure S3.3b, c, which monitor the emission of TAMRA and Cy5, respectively, when excited at their individual peak absorptions showed no sign of photobleaching. Thus, photobleaching of FAM is suspected to be the dominant source of photobleaching observed in the dynamic switching data. It should be noted that the data displayed in Figure S3.3a is a worst case scenario for FAM photobleaching in that: 1) there are no other chromophores present on the nanobreadboard to which the FAM can transfer its excitation via FRET, and 2) the FAM was continuously subjected to irradiation with no breaks, unlike in the case of all the switching and reaction kinetics data where the samples were periodically removed from the spectrofluorometer for strand injections. This perhaps explains why the observed photobleaching decay rate of 277 ± 1 minutes in Figure S3.3a is faster than those listed in Tables S3 and S4.2 for the nanobreadboards with multiple chromophores attached.

By using the above correction procedure, we are in essence taking a black box approach, such that any crosstalk and/or bleedthrough processes are assumed to be intrinsic to the system and an inherent background noise. Here, we are defining crosstalk as undesired FRET between T1/T2

and C resulting from direct excitation of T1 and/or T2 at 450 nm. Bleedthrough is defined as direct excitation of F, T1/T2, or C that produces an output signal at 668 nm. As can be seen from Figure S2.4, both crosstalk and bleedthrough should be relatively minor given: 1) the minimal overlap between the 450 nm excitation and the absorption of TAMRA and Cy5, and 2) the near lack of emission by FAM and TAMRA at 668 nm. In addition, given our "black box" approach, we are only interested in the *change* in output as a function of the input(s) added to the system, not intrinsic background signals such as crosstalk and bleedthrough. The two complicating factors mentioned above (i.e., serial dilution and photobleaching), however, are extrinsic to the system and we have therefore corrected for them as described.

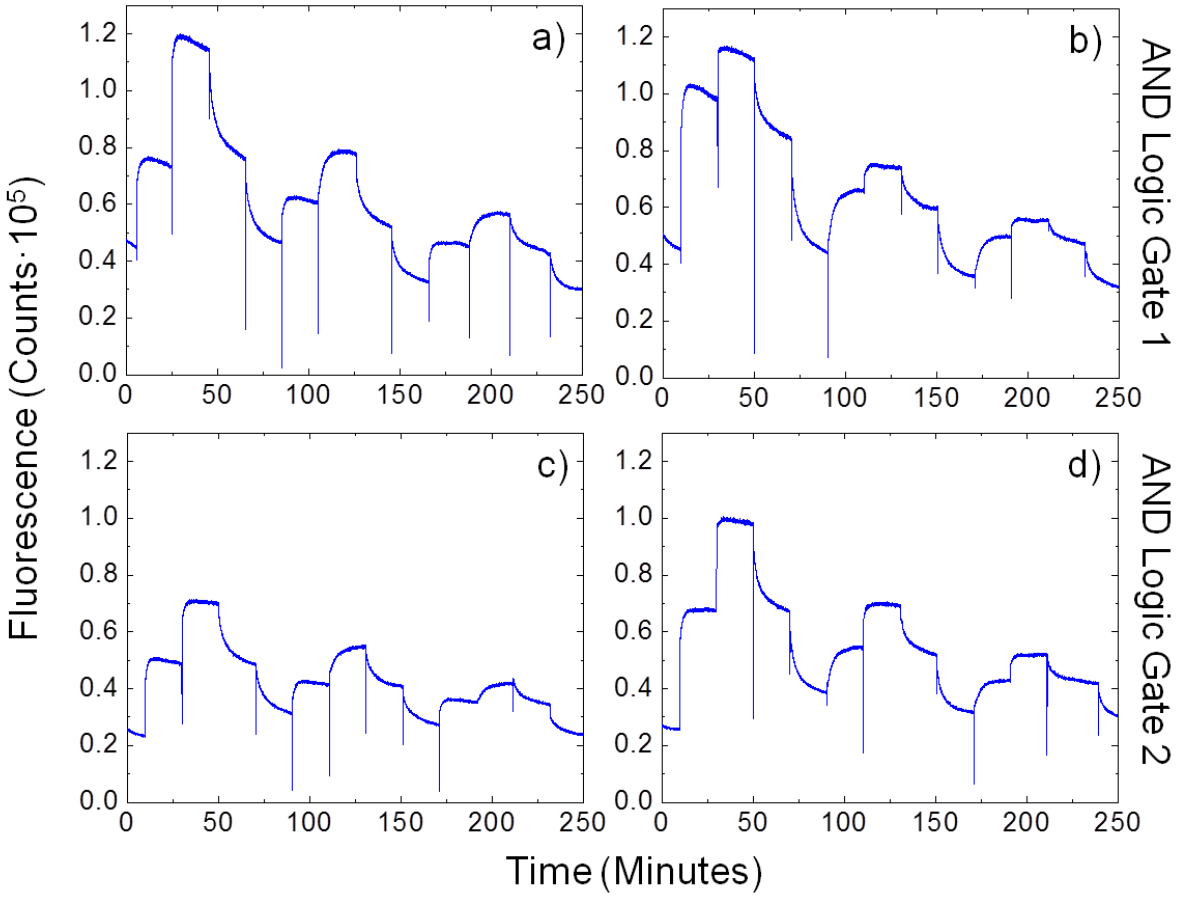

Figure S3.1: Raw (i.e., non-normalized) dynamic switching data demonstrating AND logic functionality. The fluorescence data plotted show changes in the emission of Cy5 at 668 nm arising from the addition of TAMRA, invasion and restoration strands into the sample solution while being continuously excited at 450 nm. Repeated AND logic operation by introducing **(a)** T1 to AND logic gate 1 prior to T2; **(b)** T2 to AND logic gate 1 prior to T1; **(c)** T1 to AND logic gate 2 prior to T2; **(d)** T2 to AND logic gate 2 prior to T1. Note that the vertical lines visible in the plots result from removing the sample from the fluorometer chamber to perform strand injections. A horizontal (absolute fluorescence intensity) ON-OFF threshold cannot be defined using the uncorrected data.

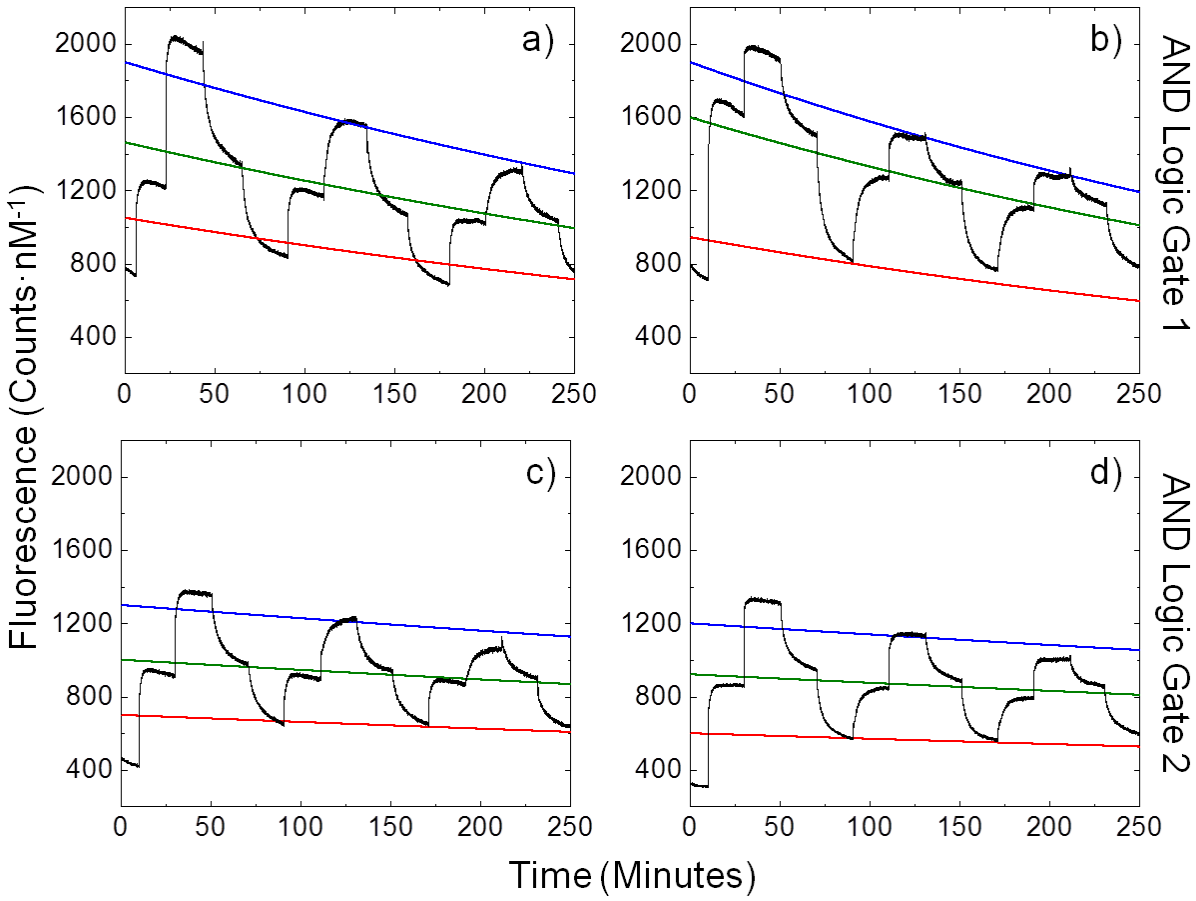

Figure S3.2: Concentration normalized dynamic switching data. Repeated AND logic operation by introducing **(a)** T1 to AND logic gate 1 prior to T2; **(b)** T2 to AND logic gate 1 prior to T1; **(c)** T1 to AND logic gate 2 prior to T2; **(d)** T2 to AND logic gate 2 prior to T1. The green curves in each plot show the single-exponential decay fit that has been used to correct the data for FRET-dependent photobleaching effects. The parameters of the fit are listed in Table S3. Note that the upper (blue) and lower (red) curves are not true "fits" to the data. They have been added to guide the eye and created by scaling the pre-exponential factor appropriately to pass through the fully ON- or fully OFF- states, respectively, without adjusting the decay (i.e., photobleaching) rate.

Table S3: Exponential fitting parameters obtained for each dynamic switching plot shown in Figure S3.2

Normalized Data	**Exponential Decay Fit Equation** $I = A_1 e^{-\frac{x}{t_1}}$		
	A_1 (Counts/nM)	**t_1 (Minutes)**	**R^2**
(**a**)	1462 ± 5	647 ± 9	0.23
(**b**)	1578 ± 5	535 ± 8	0.25
(**c**)	1001 ± 4	1754 ± 78	0.03
(**d**)	922 ± 4	1925 ± 112	0.02

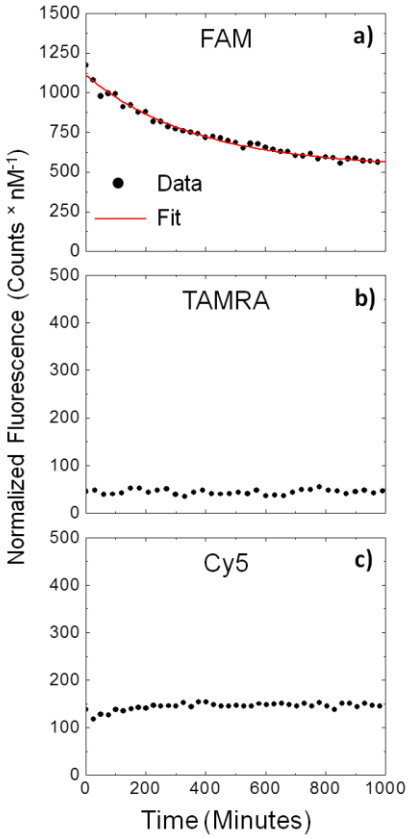

Figure S3.3: (a) Reaction kinetics data demonstrating the decrease in FAM emission with time due to degradation via photobleaching. Note that the nanobreadboards synthesized for this data set included only the FAM chromophore. The data plotted are the emission of FAM at 668 nm arising from continuous excitation at 450 nm. The data were fit to a single-exponential decay function with a time constant of 277 ± 1 minutes. Reaction kinetics data demonstrating the stability of **(b)** TAMRA and **(c)** Cy5 when continuously excited at 559 nm and 648 nm (peak absorption), respectively. Nanobreadboards were synthesized with either TAMRA or Cy5 chromophores attached and the fluorescence emission at 668 nm was monitored. The slight increase in emission observed over time in the Cy5 data is most likely a result of solvent evaporation.

SUPPORTING INFORMATION S4: *Logic Gate Switching and Reaction Rate Calculations*

To calculate reaction rate constants for the switching reactions (i.e., toehold-mediated strand displacement and DNA hybridization), dynamic switching fluorescence data were acquired in which the individual effects of T1 and T2 were observed for both logic gate designs while in the fully OFF-state (i.e., neither T1 nor T2 initially attached) by sequentially adding, invading (i.e., removing), and restoring either T1 or T2 chromophores. These dynamic switching data illustrating the individual effects of T1 and T2, normalized using the correction processing procedure described above in section S3, are shown in Figure S4.1. The data show the emission from Cy5 at 668 nm as a result of excitation of FAM at 450 nm. Invasion and restoration strands were added in stoichiometric concentrations, and then allowed to hybridize for 20 minutes. For the switching data presented in Figure S4.1, the effects of each TAMRA chromophore (i.e., T1 and T2) on each of the two logic gate designs were examined independently. The fluorescence as a function of time can be described by second-order reaction kinetics, as shown in previous work[4], and given by:

$$F(t) = F_f + \frac{F_i - F_f}{1 + k[Nanobreadboard](t - t_0)}, \quad \text{(S3)}$$

where F_i is the initial fluorescence, F_f is the final fluorescence, [*Nanobreadboard*] is the initial DNA nanobreadboard concentration, t_0 is the injection time of the specified strand and k is the reaction rate constant. To perform nonlinear curve fitting, spikes in the intensity peaks produced by removing the sample from the fluorometer chamber while performing strand injections were manually removed from the data. The reaction rates were calculated using the parameters defined in Eq. S2, with results listed in Table S4.1.

20 minute time intervals between strand injections were chosen to exceed the time to half reaction for the slowest reaction (invasion strand I1) at the concentrations used (~25 nM), which was ~13 minutes. This was to ensure that at the time of each injection well over half of the previous reaction had come to completion. For some of the faster reactions, such as the reaction between T1 and the tether which merely involves DNA duplex formation (i.e., base pairing), the rate constant is so large that the reaction is halfway to completion within less than a minute after the time of injection. In contrast, the invasion strands operate via toehold-mediated strand displacement and thus must undergo a three-way branch migration process to release T1 and T2.

The time to half reaction for this process is much longer, but is still reached relatively quickly (~3-13 minutes). Thus, although some reactions have not come to completion prior to the next injection time, the reactions all progress to a point close enough to equilibrium before the end of the 20 minute window for the system to confidently fall within the ON- or OFF- logic states.

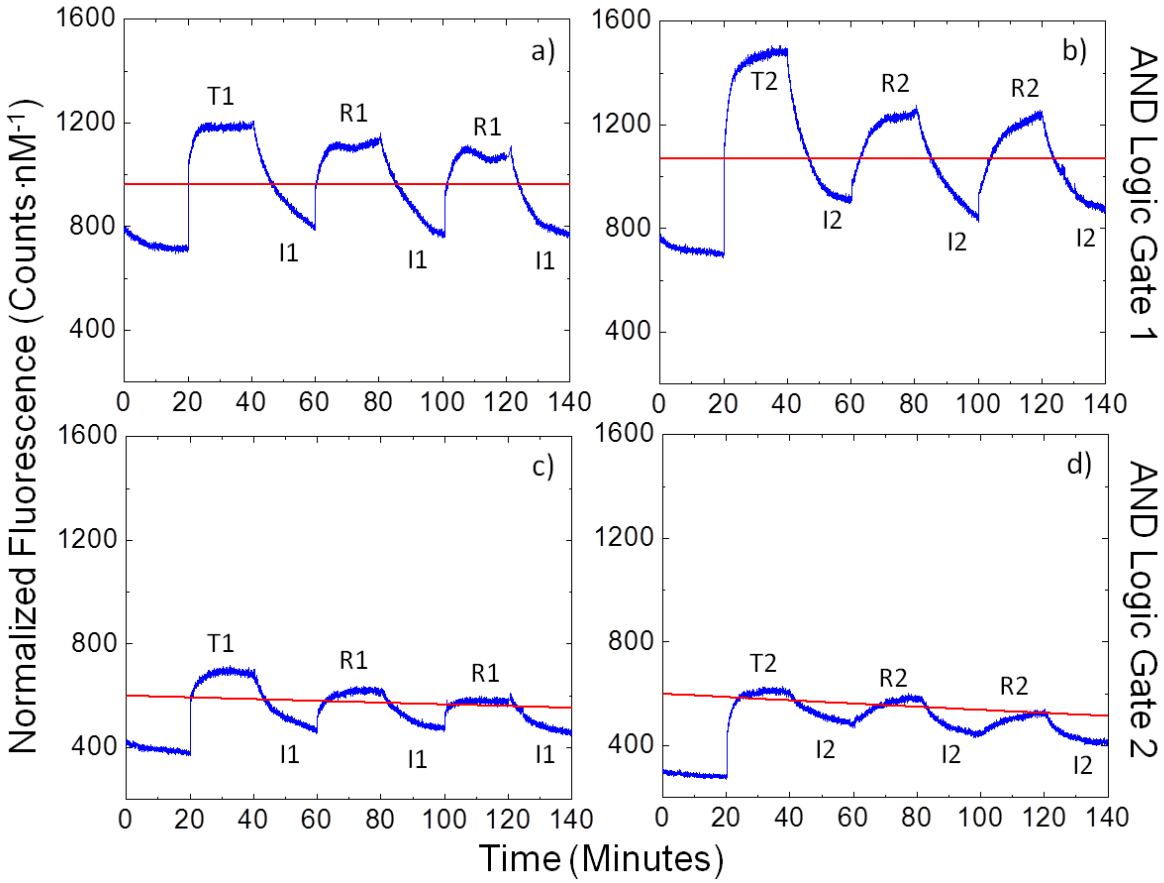

Figure S4.1: Concentration normalized dynamic switching data illustrating the individual effects of T1 and T2 on the two logic gate designs. By monitoring the effects of each logic input chromophore individually, reaction rate constants (Table S4.1) with increased accuracy can be determined and the interactions between each logic input chromophore with the nanobreadboards are not convoluted by undesired strand interactions. Data sets **(a)** and **(b)** demonstrate the effects of T1 and T2, respectively, on AND logic gate 1. Similarly, **(c)** and **(d)** examine the effects of T1 and T2, respectively, on the AND logic gate 2 design. The red curves indicate the single-exponential decay fits that are used to correct the data for FRET-dependent photobleaching effects. The fit parameters are given in Table S4.2.

Table S4.1: Second-order reaction rate constants for each logic gate design

rate constant/logic gate design	AND logic gate 1	AND logic gate 2
T1 rate constant 10^5 $(M{\cdot}s)^{-1}$	9.1 ± 0.4	10.4 ± 0.7
T2 rate constant 10^5 $(M{\cdot}s)^{-1}$	5.4 ± 0.1	7.3 ± 0.2
I1 rate constant [a] 10^5 $(M{\cdot}s)^{-1}$	0.51 ± 0.04	2.1 ± 0.3
I2 rate constant [a] 10^5 $(M{\cdot}s)^{-1}$	2.3 ± 0.9	1.4 ± 0.1
R1 rate constant [b] 10^5 $(M{\cdot}s)^{-1}$	7.6 ± 0.4	8.0 ± 0.2
R2 rate constant [b] 10^5 $(M{\cdot}s)^{-1}$	2.0 ± 0.5	1.02 ± 0.05

[a] Average rate constants from kinetics fits for three separate switching cycles.
[b] Averages calculated using kinetics data from two separate switching cycles.

Table S4.2: Exponential fitting parameters obtained for each dynamic switching plot shown in Figure S4.1

normalized data	**exponential decay fit equation** $I = A_1 e^{-\frac{x}{t_1}}$		
	A_1 (counts/nM)	**t_1 (minutes)**	**R^2**
(**a**)	9601 ± 4	$2.6\text{x}10^5 \pm 3\text{x}10^6$	0.023
(**b**)	1056 ± 1	$2.5\text{X}10^{41} \pm 3\text{x}10^{78}$	0.003
(**c**)	600 ± 4307	1727 ± 12900	0.18
(**d**)	600 ± 1557	907 ± 2546	0.72

SUPPORTING INFORMATION S5: *Logic Gate Threshold Tolerance Calculations*

The threshold tolerance, defined as the amount of error that can be tolerated by each logic gate system without compromising the device performance, were calculated after the serial dilution and photobleaching correction process were applied. Mathematically, the value is described by Eq. S4 as:

$$\tau_T = \frac{\tau_W}{\tau}, \qquad \text{(S4)}$$

where τ_W is the threshold window given in units of counts·nM^{-1} and τ is the logic threshold, also given in units of counts·nM^{-1}. Thus, the threshold tolerance τ_T is a unit less value describing logic gate performance that can be compared to data acquired from all instrument types and on different device designs. A larger threshold tolerance indicates a greater tolerance to error, and thus better device performance.

REFERENCES

[1] Horcas, I.; Fernández, R.; Gómez-Rodríguez, J. M.; Colchero, J.; Gómez-Herrero, J.; Baro, A. WSXM: A software for scanning probe microscopy and a tool for nanotechnology. *Rev. Sci. Instrum.* **2007**, *78*, 013705.

[2] Song, L.; Hennink, E. J.; Young, T.; Tanke, H. J. Photobleaching kinetics of fluorescein in quantitative fluorescence microscopy. *Biophys. J.* **1995**, *68*, 2588-2600.

[3] Zal, T.; Gascoigne, R. J. Photobleaching-corrected FRET efficiency imaging of live cells. *Biophys. J.* **2004**, *26*, 3923-3939.

[4] Graugnard, E.; Kellis, D. L.; Bui, H.; Barnes, S.; Kuang, W.; Lee, J.; Hughes, W. L.; Knowlton, W. B.; Yurke, B. DNA-controlled excitonic switches. *Nano Lett.* **2012**, *12*, 2117-2122.